ELSEVIER

Chemical Engineering Journal 70 (1998) 209–219

Chemical Engineering Journal

Aerodynamics of a novel rotating jet spouted bed

R.Y. Jumah [a,*], A.S. Mujumdar [b], G.S.V. Raghavan [c]

[a] *Department of Chemical Engineering, Jordan University of Science and Technology, PO Box 3030, Irbid 22110, Jordan*

[b] *Department of Chemical Engineering, McGill University, Montreal, Quebec, Canada H3A 2A7*

[c] *Department of Agricultural Engineering, Macdonald Campus of McGill University, Ste. Anne De Bellevue, Quebec, Canada H9X 1C0*

Received 21 April 1996; received in revised form 3 February 1998; accepted 29 April 1998

Abstract

A novel rotating jet spouted bed (RJSB) is developed and tested. It consists of a rotating air distributor with two radially located spouting air nozzles. The effects of bed height, distributor rotational speed, nozzle diameter and particle properties on the flow characteristics were examined. Various flow regimes were mapped as functions of distributor rotational speed and superficial air velocity for different materials and column dimensions. Empirical correlations were developed for the minimum spouting velocity, peak pressure drop and steady spouting pressure drop.

Keywords: Spouted bed; Rotating spouted bed; Aerodynamics; Flow regimes; Minimum spouting velocity; Pressure drop

1. Introduction

Development of more efficient solid–fluid contactors for heat/mass transfer processes, as well as chemical reactions, is important to the process industries. Efficient gas–particle contactors can be used for drying applications. Numerous modified spouted bed designs have been developed to overcome some of the limitations of the conventional spouted beds (CSBs), to accommodate the diverse properties of the materials handled, and to enhance the operability, heat and mass transfer characteristics and solid–fluid contacting efficiency [1–6]. These modifications are concerned with changes in the vessel geometry, spouting operation and mechanism, air supply, etc.

The intent of this study was to develop and investigate a novel gas–solid contacting system. The proposed contactor [1], the rotating jet spouted bed (RJSB), consists of a rotating inlet air distributor with multiple nozzles for air injection. The objectives of this study are: (i) to identify the flow regimes and the optimum operating conditions for stable spouting of the RJSBs; (ii) to gain understanding of the spouting mechanism in which the bed evolves from the packed structure into the fully developed spouting state; and (iii) to obtain general design equations to describe such flow characteristics as minimum spouting velocity, peak pressure drop, and steady spouting pressure drop as functions of the fluid–solid properties and the operating parameters of the system.

2. Experimental apparatus and procedure

A schematic diagram of the experimental set-up and the associated instrumentation is shown in Fig. 1. The rotating jet spouted bed is realized by using a rotating inlet air distributor with two radially located nozzles 2 and 3 cm in diameter, under the bed supporting screen. The nozzles, covering both the central and annular regions of the bed, are located at 4.5 and 18 cm from the center of the vessel, respectively. In the

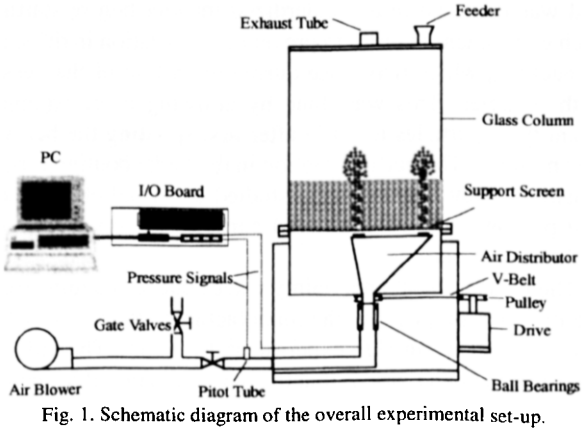

Fig. 1. Schematic diagram of the overall experimental set-up.

* Corresponding author. Fax: +962-2-295123; E-mail: ramy@just.edu.jo

1385-8947/98/$ - see front matter
PII S1385-8947(98)00091-6

Table 1
Dimensions of bed particles

Material	$L\times10^3$ (m)	$B\times10^3$ (m)	$Z\times10^3$ (m)	D_{Pe}[a] $\times10^3$ (m)	D_{Pgm}[b] $\times10^3$ (m)	D_p[c] $\times10^3$ (m)	ϕ[d] (−)
Polystyrene	3.32	3.00	2.27	3.50	2.82	2.98	0.85
Polyethylene	4.11	3.46	3.28	4.45	3.59	3.90	0.88
Soybean	8.22	6.96	5.97	8.67	6.99	7.37	0.85
Corn	9.05	8.32	6.35	9.67	7.80	8.35	0.86

[a]Equivalent spherical diameter.
[b]Geometric particle diameter $=(L\times B\times Z)^{1/3}$ [7].
[c]Effective particle diameter $=D_{Pe}\times\phi$.
[d]Sphericity $=D_{Pgm}/L$ [7].

preliminary experiments, a smaller nozzle size (1 cm in diameter) was tested and the observations show a very high pressure drop and poor flow distribution. This directed us to use larger nozzles (2 and 3 cm in diameter) in the entire work. In addition, equal sizes for both the central and annular nozzles was used during each experiment. The distributor is enclosed within a perfectly sealed aluminum box. The rotating section of the main inlet air pipe is provided on its outer surface with two rubber-sealed ball bearing assemblies; all are circumfused by another well sealed coaxial pipe. The downstream part of this rotating section is engaged with two belt-driven pulleys connected to a 3-hp variable speed AC motor using an AC inverter.

The spouted bed consists of a flanged cylindrical glass vessel 45 cm diameter and 90 cm in height. The whole assembly of the vessel, distributor, and drive was carefully leveled and securely mounted on a rigid metallic frame. The spouting air is supplied by a high-pressure blower. The air flow rate is measured with a precalibrated pitot tube and regulated by means of gate valves on the feed and bypass lines. Differential pressure drop across the pitot tube is measured using a manometer or a pressure transducer. Pressure drop across the bed is measured using static pressure taps connected to a calibrated differential pressure transducer. The analog signals for various sensors are acquired by a data acquisition system connected to a personal computer for digitized data gathering.

Seed quality corn, soybean, polyethylene, and polystyrene were used as test materials. Dimensions and physical properties of the particles tested are given in Tables 1 and 2. The bed was prepared in a standardized manner before starting each experiment in order to prevent any variation in the state of packing, which may arise during the filling of the vessel with particles. This was done by allowing a pre-weighed quantity of particles to settle after first spouting the bed for few minutes. The particle motion in the bed, spouting mechanism and flow regimes were studied by visual observation and photography using colored particles in contrast to the main bulk of particles.

The measurement uncertainty values due to random errors are the ones supplied by the manufacturers or are estimated from a 'single-sample' experiment [11–13]. The rule of thumb in the latter case is that the maximum possible error is equal to plus or minus half the smallest scale division (the least count) of the instrument. Table 3 lists the estimated experimental uncertainty values for both measured and calculated variables.

To investigate the reproducibility of the results in the system, two replicates were made for all the flow experiments. From these tests, the reproducibility of U_{ms}, ΔP_s and ΔP_M were at ±2%, ±3% and ±11%, respectively [1]. The relatively high nonreproducibility in ΔP_M is related to the fact that the peak pressure drop is a function of the initial structure of the bed. Nevertheless, the results obtained confirmed good reproducibility of the results compared to the usually observed lack of ΔP_M reproducibility in conventional spouted beds. This could be attributed to the new and enhanced flow system developed in the contactor as a result of the of the

Table 2
Physical properties of bed particles

Material	ρ_s (kg/m^3)	ρ_b (kg/m^3)	Ar (−)	U_t[a] (m/s)	U_{mf}[a] (m/s)	ε[b] (−)
Polystyrene	1020.0	666.6	8.18×10^5	5.90	0.99	0.35
Polyethylene	914.1	579.9	1.64×10^6	6.75	1.12	0.36
Soybean	1237.9	733.2	1.50×10^7	10.37	1.91	0.41
Corn	1226.4	783.2	2.17×10^7	11.32	2.04	0.36

[a]U_t and U_{mf} are calculated values [8–10].
[b]$\varepsilon=1-(\rho_b/\rho_s)$.

Table 3
Experimental uncertainty for measured and calculated variables

Variable	Uncertainty
Superficial velocity, U	±2.77%
Pressure drop, ΔP	±0.32%
Particle diameter, D_p	±0.40%
Particle density, ρ_s	±1.35%
Bed density, ρ_b	±1.35%
Particle sphericity, ϕ	±0.43%
Particle terminal velocity, U_t	±1.04%
Bed voidage, ε	±2.86%
Rotational speed, N	±0.75%
Ar	±2.88%
Re_{ms}	±3.14%
H/D_c, D_n/D_c, D_p/D_c	±1.57%
$\Delta P/\rho_b gH$	±1.52%
V_θ/U_t	±1.70%

rotary action of the nozzles and the fact that the distributor rpm is a main process factor in addition to the bed conditions.

3. Results and discussion

3.1. Flow regime diagrams

As in conventional spouted beds [2], spouting in a rotating spouted bed is a visually observable phenomenon that occurs over a definite range of gas velocity for a certain combination of gas, solids and equipment geometric and physical parameters. The parameters of interest are: gas flow rate, particle size and shape, particle density, gas inlet nozzle size, bed height and distributor rotational speed. When the rotational speed, N, of the air distributor is increased, the bed may be in different states at the same gas superficial velocity, U. Consequently, the studies of flow regimes for different material-vessel combinations are presented in N–U coordinates. Fig. 2 shows examples of such flow regime diagrams for both polyethylene and corn particles representing two ranges of particle size and density. These flow diagrams were obtained starting with the rotational speed at zero speed and then gradually increasing the gas flow rate to obtain the onset of spouting. The gas flow rate was then kept constant while gradually increasing the rotational speed until the disappearance of the characteristic form of the spouted bed, and thus the development of another flow regime. This procedure was repeated for different values of the gas superficial velocity beyond the value required to initiate steady and stable spouting. Three distinct flow regimes were observed within the operating parameter ranges studied.

3.1.1. Full rotating spouting

Depending on the bed height, nozzle size and particles used, at low rotational speeds, stable spouting occurs in both central and annular regions of the bed over the entire range of gas superficial velocities higher than the incipient spouting velocity.

First, for a stationary air distributor ($N=0$), two individual cells are formed each with its own annulus with more vigorous agitation and circulation inside the bed than the equivalent single-spout bed, but at the expense of higher gas consumption and the presence of dead zones surrounding the spouting cells. This might be attributed to the flat geometry of the supporting grid.

On the other hand, with the rotating air distributor, a completely different gas–particle dynamics is established. The particles at the base of the bed receive a sudden impulse from one of the incoming rotating jets and accelerate from rest to their maximum velocity as result of the frictional drag of the high velocity ascending air jet, and then decelerate until they reach zero velocity at the top of the fountain(s), where they reverse their direction of movement and fall back into the bed surface. A temporary active cell in the bed assumes a loose packed orientation when the air jet is periodically and continuously relocated to the following sections of the bed. However, particles from the layer surrounding other active cells continuously percolate towards the rotating core in both axial

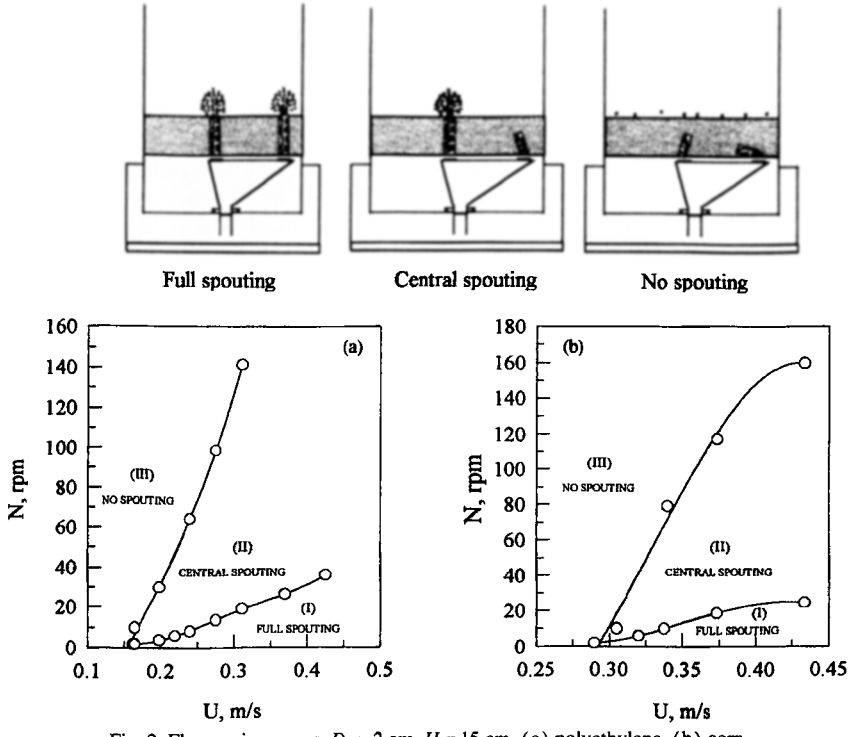

Fig. 2. Flow regime maps, $D_n=2$ cm, $H=15$ cm. (a) polyethylene, (b) corn.

radial directions, creating continuous motion in the entire bed cross-section.

Depending on the gas flow rate and distributor rotational speed, particles of different size and density have different trajectories within the spouts and fountains; hence, different radial and angular landing positions on the bed surface. Large and heavy particles like corn and soybeans tend to land more frequently at smaller positions and hence execute a higher proportion of cycle time than small and light particle like polyethylene and polystyrene.

This regime clearly shows such spouted bed features as particle circulation, an ascending particle flow in the active spout region and downward–inward flow in the local annulus surrounding the rotating spout in both the central and annular regions of the bed. Moreover, this flow regime is characterized by certain distinct features.

(i) The distributor rotation causes the jets and hence the entrained solid particles to deviate in the opposite angular direction with respect to the nozzle opening and this results in a rotating sprinkler-like distribution of the solids over the periphery of each cell. This phenomenon is more pronounced in the case of the second jet covering the annular section of the bed because of its larger radius of rotation and hence higher angular velocity.

(ii) Intensive systematic particle circulation and hence short contact time between the solid particles and the gas with fast solids turnover.

(iii) The cyclic rotation of the spouts causes intensive mixing of the particles and their exchange between the rotating spouting cells and prevents dead zone formation in spite of the fact that the bed support screen is flat.

3.1.2. Rotating central spout-pulsating annulus

If the rotational speed is high, the jet emerging from the second nozzle covering the annulus region of the bed cross-section with its larger radius of rotation, R, compared with the central jet, will have a higher circumferential velocity ($V_\theta = 2\pi RN$) and higher frequency of gas relocation. This produces an increase in the slope or deviation of the air jet from the vertical direction contributing to significant shear stresses and resistance forces in the direction of gas penetration proportional to the jet circumferential velocity. In such a case, the annular spout will loose its kinetic energy and collapse leaving annulus region in a no-spouting condition with local pulsation due to the internally rotating spout. This results in a second flow regime characterized by an external rotating central spouting and an internal rotating annular spouting with local bed pulsating. The solids circulation is significantly reduced compared to the first flow regime because most of the particles are in a nearly loosely packed pulsating state with periodic aeration with only 20–25% of the solid material (depending on the nozzle diameter, flow rate and rpm) in the rotating central spouting region. This causes a reduction of the time-averaged voids in the bed.

The effect of particle oscillation in the annulus region along with the rotating action of the central region causes continuous transfer and rolling of particles from the surrounding sloped cone-shaped layers towards the core section. It is worth noting that this flow regime possesses some features of the spout-fluid bed; gas passes through the bed as a central rotating jet and a pulsating annulus locally fluidized/aerated by the spent gas from the second rotating nozzle.

The gas and particle flow patterns in this flow regime lead to the hypothesis that both the magnitude and the direction of the momentum at the gas inlet are the governing parameters, and that the vertical fluid drag is a monotonously decreasing function of the rotational speed. Hence, the state of dynamic equilibrium between the various forces acting on the spout–annulus interface that keep the spout stable in shape and direction does not exist. The resultant effect of this high rpm and the resulting resistances leads to the conclusion that while the spout is still developing, the gas jet is relocated; thus, this spout will never pierce the annulus region of the bed even at a high gas flow rate, and this will create an annular internal cavity inside the bed.

3.1.3. No spouting

Above a rather high rotational speed (depending on the air flow rate, bed height, and particle properties), the central spout also collapses; the bed starts to oscillate in all directions, and the main body of the gas forms a vortex flow with its mouth directed toward the central region. In this flow regime, because of bed inertia and particle interaction, the spouting air percolates through the bed in a vertical direction bringing the particles into local pulsation; hence, the entire bed attains a 'pseudo-fluidized' state.

A critical analysis of the flow regime diagrams shows that the full rotating spouting regime (regime I) is the most effective operating regime in terms of bed aerodynamics, and consequently performance in heat and mass transfer applications. This is because of the lower rpm and hence lower power requirements, more stable and uniform gas distribution, the systematic particle circulation across the entire bed, and hence more vigorous mixing of particles. For these reasons, the discussion in the following sections will concentrate on experiments at low rpm values ($N < 14$ rpm).

3.2. Spouting mechanism

Generally, the spouting mechanism in which the bed of particles changes from a packed state to fully developed spouting is best described with reference to plots of bed pressure drop vs. superficial gas velocity. In order to generalize the analysis, the pressure drop and superficial gas velocity are written in dimensionless form, i.e., $\Delta P/\rho_b g H$ and Re. The former represents the ratio between the bed pressure drop and the bed weight per unit cross-sectional area while the latter represents the particle Reynolds number. Fig. 3 shows typical dimensionless pressure drop evolution traces for polyethylene particles at 0, and 10 rpm. The plots are supplemented by branches illustrating the reverse process, that is, the col-

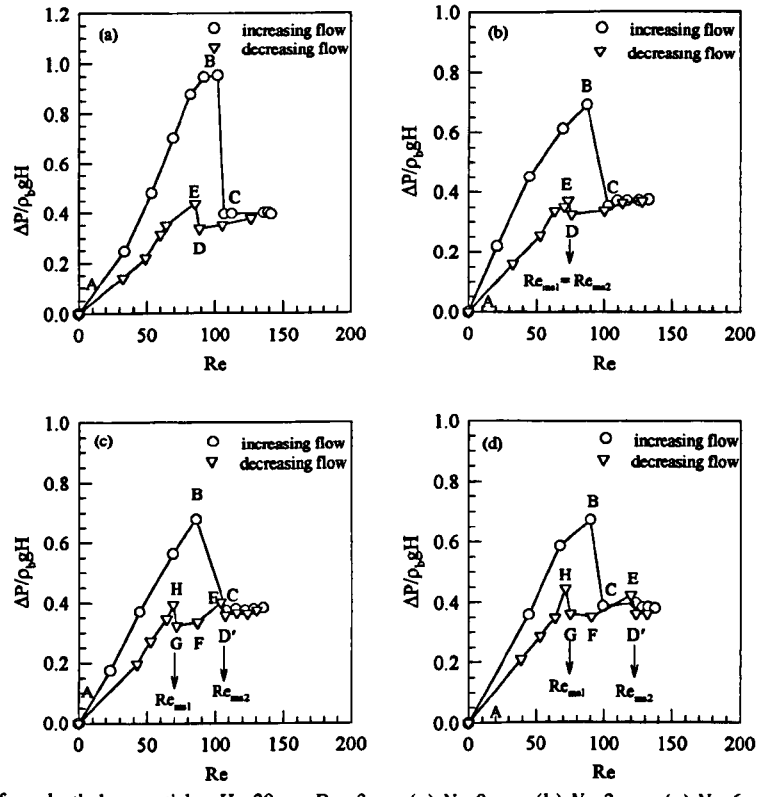

Fig. 3. Spouting characteristics for polyethylene particles, $H=20$ cm, $D_n=3$ cm. (a) $N=0$ rpm, (b) $N=2$ rpm, (c) $N=6$ rpm, (d) $N=10$ rpm. B: maximum spouting pressure drop; C: onset of spouting; D: minimum spouting condition; D': annular minimum spouting E: central and annular spout collapse; E: annular spout collapse; F: central spout active; G: central minimum spouting; H: central spout collapse.

lapse of both central and annular spouts on decreasing the gas flow rate.

The following sequence of events is observed as the flow rate is increased.

3.2.1. Increasing air flow

Curve A→B: As in conventional spouted beds, the pressure drop increases almost linearly with increasing gas flow rate while the fixed-bed state remains unchanged. For stationary air distributor (Fig. 3), two small cavities and two internal spouts are formed. When the air distributor rotates (Fig. 3b,c,d), two internally relocated annular cavities are formed along the path of the rotating internal spouts. An arch of compacted particles that offers high resistance to flow exists above the internal spouts so that the pressure drop rises until it reaches a peak value at point B.

Curve B→C: Beyond point B, the height of the internal spouts increases and the stationary or rotating jets have enough momentum to pierce the bed surface and hence spouting begins. Therefore, the pressure drop suddenly decreases to point C.

Curve beyond C: Both spouts are fully developed and the pressure drop remains nearly constant.

3.2.2. Decreasing air flow

Two different spout termination mechanisms were observed. In the case of stationary distributor and very low rotational ($N=2$ rpm) speeds, the trend is similar to that found for conventional spouted beds. While the gas flow rate is decreased, the pressure drop remains nearly constant and the bed remains in the spouting state until point D is reached; this represents the minimum spouting condition for both central and annular spouts (U_{ms} or Re_{ms}). A slight reduction of the air flow rate causes the spouts to collapse and the pressure drop to rise suddenly to point E.

When the rotational speed is higher (Fig. 3c,d) the annular spout collapses at a higher superficial velocity than the central one. This may be attributed to the fact that the annular spout has a higher velocity component in the angular direction because of its larger radius of rotation; hence, larger deviation of the spout from the vertical direction. The spout failure locations are represented in Fig. 3c,d by points D', E, F, G and H. Point D' represents minimum spouting conditions for annular spout (U_{ms2} or Re_{ms2}), point G represents minimum spouting conditions for central spout (U_{ms1} or Re_{ms1}), point F designates the state when the central spout is still active and points E and H represent the secondary peaks after failure of the spouts.

3.3. Minimum spouting velocity

A spouted bed is characterized by its minimum flow requirement since a minimum air velocity is required for spouting. The minimum spouting velocity, U_{ms}, depends on the properties of the bed material and of the spouting agent, the bed height, and system geometry. Another added factor in the rotating jet spouted bed is the angular velocity of the air distributor. Experimental values of U_{ms} are determined at the point where the spouts collapse as the air flow rate is decreased. Using dimensional analysis and multiple nonlinear regression, the following empirical equations for the minimum spouting condition were derived:

$$Re_{mso}=0.68\left(\frac{H}{D_c}\right)^{0.98}\left(\frac{D_n}{D_c}\right)^{0.82}Ar^{0.54} \quad (1)$$

$$Re_{ms1}=0.59\left(\frac{H}{D_c}\right)^{1.02}\left(\frac{D_n}{D_c}\right)^{0.91}Ar^{0.57}\left(\frac{V_{\theta 1}}{U_t}\right)^{0.01} \quad (2)$$

$$Re_{ms2}=8.46\left(\frac{H}{D_c}\right)^{0.83}\left(\frac{D_n}{D_c}\right)^{1.08}Ar^{0.45}\left(\frac{V_{\theta 2}}{U_t}\right)^{0.11}. \quad (3)$$

These correlations are valid for:

H/D_c	0.222–0.444
D_n/D_c	0.044–0.0667
Ar	8.18×10^5–2.17×10^7
$V_{\theta 1}/U_t$	0–8.0×10^{-3}, and
$V_{\theta 2}/U_t$	0–3.2×10^{-2}

Eq. (1) represents the minimum spouting condition for the case of a stationary air distributor ($Re_{ms1}=Re_{ms2}=Re_{mso}$) while Eqs. (2) and (3) represent minimum spouting conditions for the case of rotating air distributor for the central region spout and annular region spout, respectively. The correlations could predict the experimental data with a standard deviation less than 6, a standard error of fit less than 10 and a correlation coefficient (r^2) higher than 0.98. $V_\theta(=2\pi RN)$ represents the nozzle circumferential velocity, R is the radius of rotation and N is the rotational speed in revolution per second. The correlations developed are based on groups typically used in spouted bed literature and the statistical analysis made confirms the system performance [1].

Fig. 4 presents examples of the variation of Re_{ms1} and Re_{ms2} with dimensionless bed height for different particles (different Ar). The data for all particles show that U_{ms} and hence Re_{ms} increases almost linearly as the static bed height is increased. The deeper the bed the larger the amount of air needed to keep the central or annular bed regions at spouting condition and therefore the higher is U_{ms}. It is important to note that, unlike conventional spouted beds, the rotating jet spouted bed permits spouting of shallow beds as low as 10 cm (that is, $H/D_c=0.22$). Conventional spouted beds with low bed depths ($H/D_c<1$) exhibit poor quality of solids mixing and circulation and the greater part of the gas flow is localized around the spout [14,15].

The effect of the distributor rotational speed in terms of the dimensionless circumferential velocities, $V_{\theta 1}/U_t$ and $V_{\theta 2}/U_t$ on their corresponding Re_{ms} is presented in Fig. 5 for $D_n/D_c=0.067$ and $H/D_c=0.22$ using different particles. Increasing $V_{\theta 1}/U_t$ from zero produces a slight decrease in both Re_{ms1} and Re_{ms2}. Further increases in the circumferential velocity show increases in Re_{ms2} while Re_{ms1} remain virtually constant. The small reduction in Re_{ms} when N is increased from zero might be explained by the pulsating action of the rotating jets, which helps enhance the effectiveness of the spouting air streams. However, further increase in N introduces the effect of the resistance forces discussed earlier that tend to deviate the air jets from the vertical direction (particularly the annular jet); thus, more flow is required to maintain stable spouting and consequently higher Re_{ms2} values.

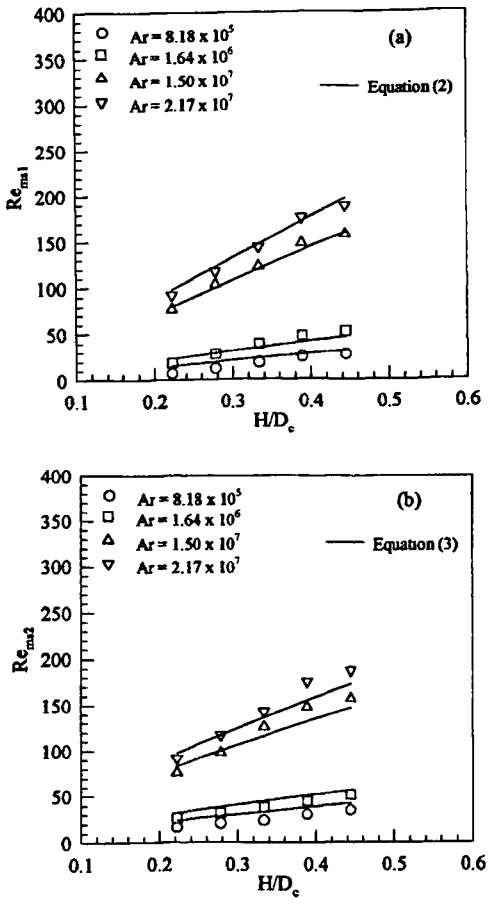

Fig. 4. Effect of dimensionless bed height on (a) Re_{ms1} and (b) Re_{ms2}. $D_n/D_c=0.0444$, $N=2$ rpm.

Additional light was shed on the dynamic behavior of the RJSB by examining the effect of particle properties viz. diameter, shape, and density on the minimum spouting velocity. These properties along with the fluid properties are often combined into a single parameter—the Archimedes number Ar, which represents the ratio between gravity forces and viscous forces. The effect of this parameter on Re_{ms} is depicted in Fig. 6 for different H/D_c ratios using $D_n/D_c=0.044$ and $N=6$ rpm. The main trend is for both Re_{ms1} and Re_{ms2} to increase with Ar. One possible explanation for this behavior is that materials with large Ar, in this case corn

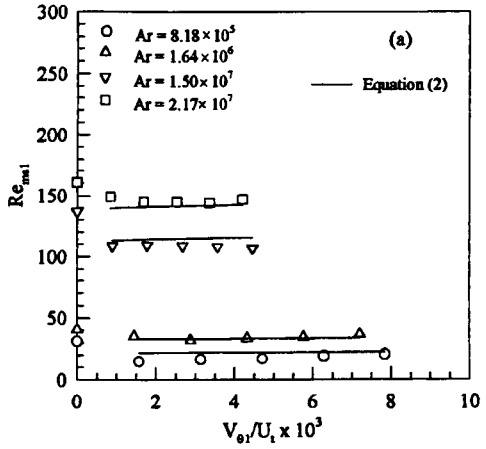

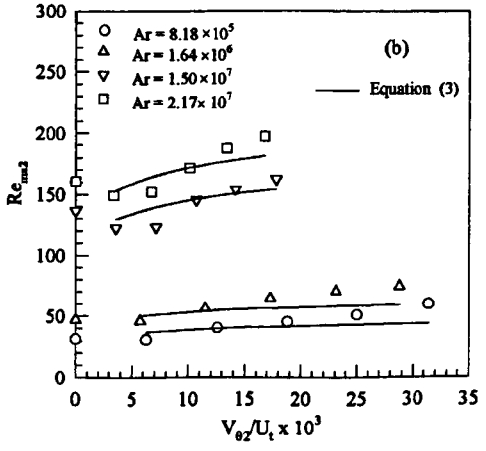

Fig. 5. Effect of dimensionless circumferential velocity on (a) Re_{ms1} and (b) Re_{ms2} for different Ar, $D_n/D_c = 0.0667$, $H/D_c = 0.22$.

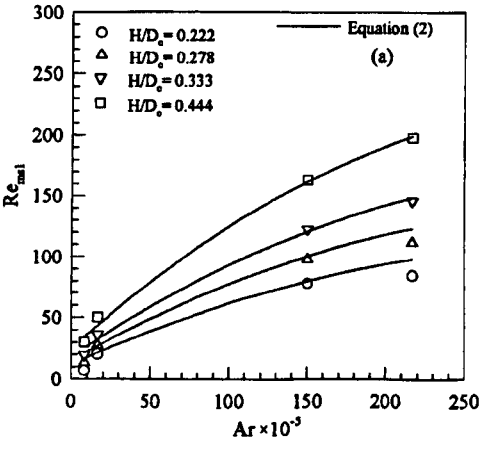

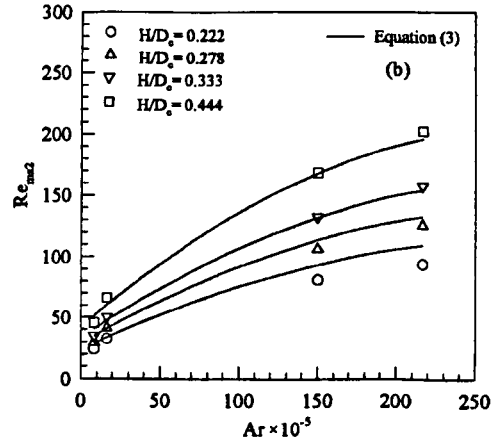

Fig. 6. Effect of Archimedes number on (a) Re_{ms1} and (b) Re_{ms2} for different H/D_c values, $D_n/D_c = 0.0444$, $N = 6$ rpm.

and soybeans, offer more resistance to flow than polystyrene and polyethylene (lower Ar). Large and heavy particles have large mass (inertia) and respond slowly to the change in fluid flow while small and light particles generally follow more closely the changes in fluid motion. Therefore, gravity forces are more significant than viscous forces for large particles under spouting conditions.

To examine the effect of nozzle diameter, several experiments were performed using two different nozzle sizes for different solid materials and distributor rotational speed. The results obtained are presented as Reynolds number vs. dimensionless nozzle circumferential velocity with the dimensionless nozzle diameter as a parameter (Fig. 7). Evidently, the particle Reynolds number for both spouting cells increases as the dimensionless nozzle diameter increases from 0.044 to 0.067. This increase is due to the larger spout diameter and hence larger active cross-sectional area causing higher air flow requirements for transporting an increased volume of particles through the active spouting cells and for preserving stable dynamic conditions. Note that the difference is more pronounced at higher Archimedes numbers.

From the practical point of view, use of larger nozzle size is recommended (i.e., $D_n = 3$ cm or $D_n/D_c = 0.067$), since at high air velocity the nozzle pressure drop increases significantly with decreasing the nozzle diameter, and therefore increases the pumping power requirements. Also, using a small nozzle diameter limits the contact between air and particles because of the smaller active spouting area and higher air velocity.

3.4. Pressure drop

As in conventional spouted beds, two pressure drop values are of practical interest in the design and operation of the rotating jets spouted bed, namely the peak pressure drop ($-\Delta P_M$) and the steady (fully developed) spouting pressure drop ($-\Delta P_s$). These values are represented by the following empirical correlations:

$$\frac{\Delta P_M}{\rho_b g H} = 2.12\left(\frac{H}{D_c}\right)^{0.47}\left(\frac{D_n}{D_c}\right)^{0.27} \quad (4)$$

$$\frac{\Delta P_s}{\rho_b g H} = 0.63\left(\frac{H}{D_c}\right)^{0.12}\left(\frac{D_n}{D_c}\right)^{0.16} \quad (5)$$

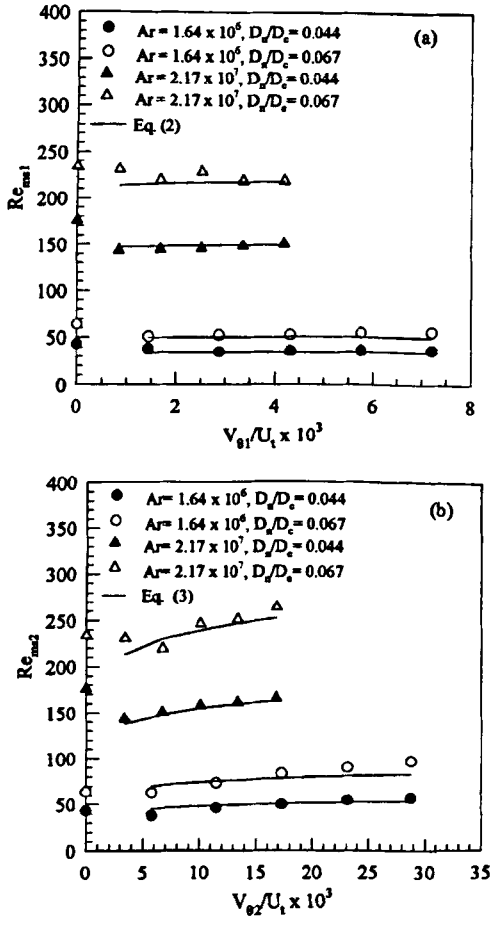

Fig. 7. Effect of dimensionless nozzle diameter on (a) Re_{ms1} and (b) Re_{ms2}, $H/D_c = 0.333$.

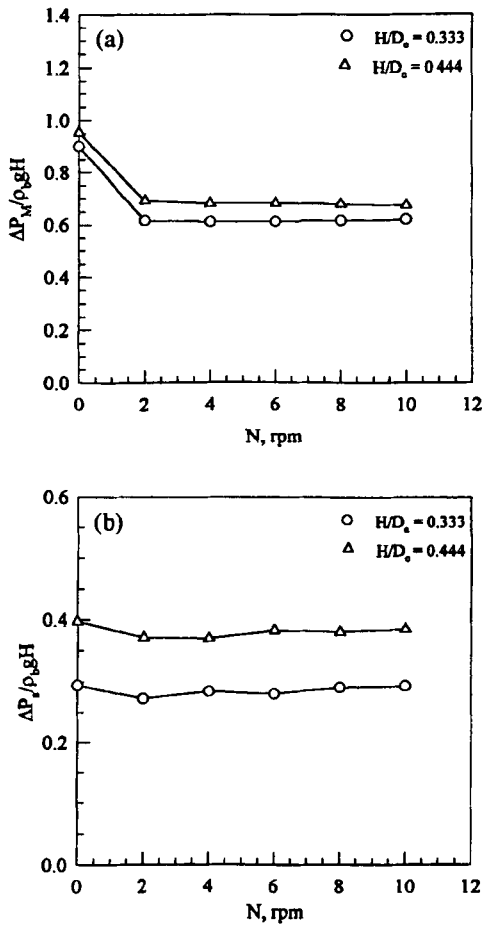

Fig. 8. Effect of rotational speed on (a) dimensionless peak pressure drop and (b) dimensionless steady spouting pressure drop for polyethylene particles, $D_n/D_c = 0.0667$.

The correlations predict the experimental data with a standard deviation less than 0.01, a standard error less than 0.02 and a correlation coefficient (r^2) higher than 0.97. These correlations are valid within the same ranges of parameters as the minimum spouting velocity correlations (Eqs. (1)–(3)).

Fig. 8 shows the effect of distributor rotational speed, N, on the peak pressure drop and steady spouting pressure drop, respectively, for two bed heights of polyethylene particles. These figures show that neither the peak pressure drop nor the steady spouting pressure drop are affected by the rotational speed. It is clear, however, that the values for stationary distributor ($N = 0$ rpm) are slightly higher, especially for the dimensionless peak pressure drop which approximately approaches unity. The lower pressure drop values for $N > 0$ can be attributed to the pulsation and shaking actions introduced by the internal rotating jets. This causes disturbance in the stable packed bed structure by destroying the interparticle forces before the onset of spouting. Similar behavior was observed for beds of polystyrene, corn, and soybeans particles.

In order to analyze the effect of the geometric parameters of the contactor, the values of the dimensionless pressure drop, $\Delta P_M/\rho_b gH$ and $\Delta P_s/\rho_b gH$, are plotted in Fig. 9 against the dimensionless bed height (H/D_c) for different dimensionless effective particle diameters (D_p/D_c) with the dimensionless nozzle diameter (D_n/D_c) as parameter. Both pressure drop values tend to increase with dimensionless bed height irrespective of the solid material; the effect is more pronounced on the peak pressure drop. It can be noticed that as the inlet air nozzle size increases, the pressure drop increases. These figures also show a comparison between the experimental data and the calculated values using Eqs. (4) and (5). This demonstrates that the agreement is good.

For the shallow bed heights ($H/D_c < 1$) used in this work, the ratio of the peak pressure drop to that across a comparable fluidized bed at minimum fluidization,

$$\Delta P_{mf} = (1-\varepsilon)(\rho_p - \rho_g)gH = \rho_b gH \quad (6)$$

is considerably less than unity for all dimensionless bed heights. In a conventional spouted bed, the peak pressure drop may be several times the bed weight per unit area [2,3], i.e.,

$$\Delta P_M = k\Delta P_{mf} \quad (7)$$

where $k = 1$ to 3. The difference between the results obtained

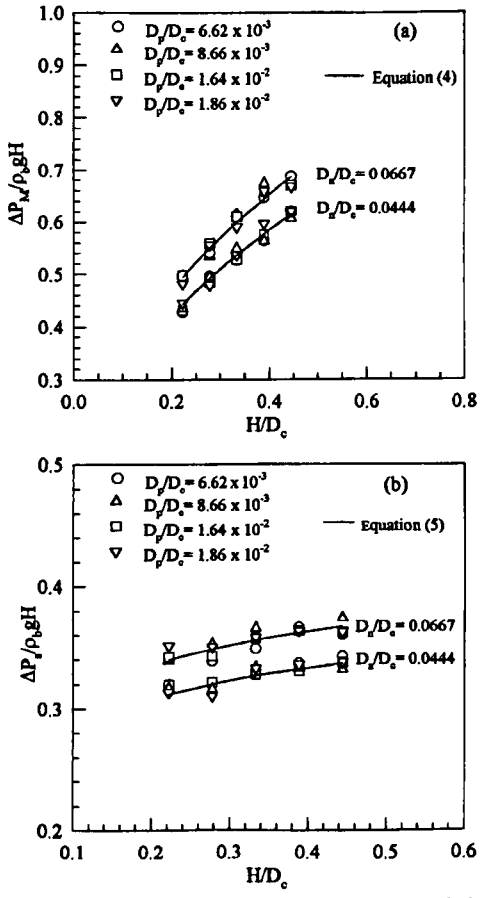

Fig. 9. Variation of (a) dimensionless peak pressure drop and (b) dimensionless steady spouting pressure drop with H/D_c and D_n/D_c for different D_p/D_c, $N>0$.

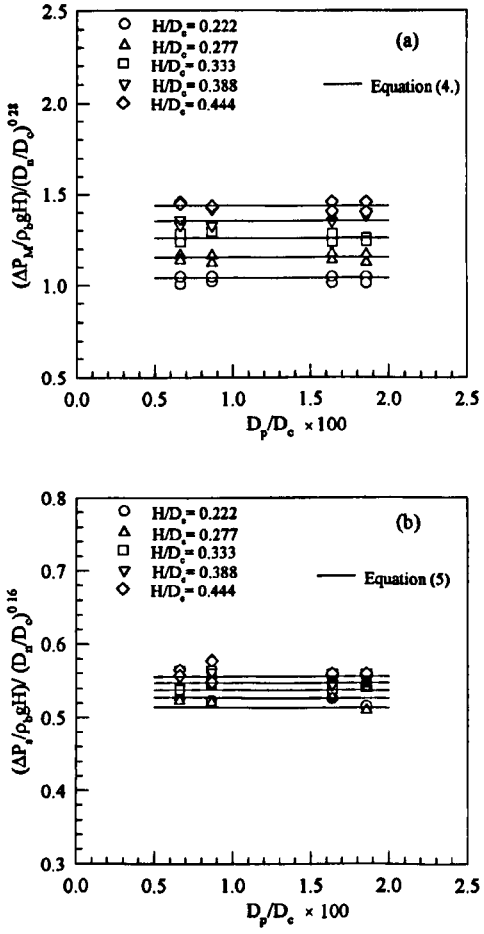

Fig. 10. Variation of (a) $(\Delta P_M/\rho_b gH)/(D_n/D_c)^{0.28}$ modulus and (b) $(\Delta P_s/\rho_b gH)/(D_n/D_c)^{0.16}$ modulus with D_p/D_c for different H/D_c, $N>0$.

in this study and the values predicted by Eq. (7) highlights the impact of the rotating jets upon the spouting mechanism and, in particular, upon the bed structure before the onset of spouting. It should be noted also that the flat geometry of supporting grid and the periodic relocation of the spouting jets beneath, play an important role in lowering the peak pressure drop. Hence, the entire bed is not supported by the rising rotating jets; it is supported, in part by the bottom screen or the walls. This means that the entire pressure drop at the air side can approach the pressure drop at the spouts themselves, which is known to be much smaller than the pressure drop caused by the entire bed. On the other hand, the pressure drop, ΔP_s across a fully developed spouted bed is always lower by at least 60% than that required to support the weight of the bed. It was observed that the periodic relocation of the spouting jets helps to avoid any pressure difference problems normally noticed in conventional spouted beds, i.e., stationary nozzles as a result of feeding both nozzles from same air flow.

To analyze the effect of particle diameter, the dimensionless pressure drop parameters are further normalized by the (D_n/D_c) modulus obtained from the empirical Eqs. (4) and (5); thus, the effect of dimensionless nozzle diameter is eliminated as shown in Fig. 10. These plots demonstrate that the particle diameter has little or no effect on the pressure drop values and this can be explained by the fact that the bulk density and hence the bed weight is the most influential parameter on the pressure drop among other particle-related properties and this factor is already included in the pressure drop modulus, $\Delta P/\rho_b gH$. This is in agreement with the empirically estimated figures.

4. A note on the spouting stability and scale-up

For conventional spouted beds, Becker [14] demonstrated that the critical value of the ratio D_c/D_n is 3. Ghosh [16] proposed that fine particles can be spouted as long as the ratio D_n/D_p does not exceed 30, while Chandnani and Epstein [17] indicated that D_n/D_p should be less than 25. Németh et al. [3] and Pallai et al. [4] stated that the optimum ranges for the ratios D_n/D_p, D_c/D_p, and D_c/D_n are 3–30, 25–200, and 6–10, respectively. The ratios D_n/D_p, D_c/D_p, and D_c/D_n employed in this study are listed in Table 4. The table also

Table 4
Expected stability of single nozzle spouting for the different nozzle and particle diameters used in the present study

D_p (mm)	D_n (mm)	D_n/D_p	D_c/D_n	D_c/D_p
2.981	20	6.71 ✓	22.5 ×	150.98 ✓
2.981	30	10.07 ✓	15.0 ×	150.98 ✓
3.898	20	5.13 ✓	22.5 ×	115.44 ✓
3.898	30	7.69 ✓	15.0 ×	115.44 ✓
7.367	20	2.71 x	22.5 ×	61.08 ✓
7.367	30	4.07 ✓	15.0 ×	61.08 ✓
8.354	20	2.39 x	22.5 ×	53.86 ✓
8.354	30	3.59 ✓	15.0 ×	53.86 ✓

✓: stability criteria satisfied.
×: stability criteria not satisfied.

shows if the spouting criteria discussed above are achieved or not. It is clear from the table that stable spouting would not have been achievable if a single nozzle was used in the study. It is demonstrated also that D_c/D_n is higher than the upper limit required for stable spouting by 50 to 125%.

The condition that the ratio D_c/D_n must be in the range 6 to 10 would also imply a maximum bed diameter of respectively 20 and 30 cm for the 2 and 3 cm nozzle diameters used in this study for stable spouting from a single nozzle. Noting that the column diameter (D_c) used in this study is 45 cm, It is obvious that it was possible to more than double the column diameter in the RJSB (with two nozzles) without any instability problems compared to the conventional spouted bed with only one stationary inlet nozzle. This gives another advantage of the RJSB in terms of capacity, efficiency, and scale-up. It is worth to point out at this point that the system developed in this study has been successfully used for drying grains using both continuous and intermittent (on/off) spouting and heating schemes [18]. The results indicate that the drying kinetics are comparable with conventional spouted and fluidized beds for slow drying materials when the drying rate is controlled by internal diffusion.

5. Conclusions

The following conclusions are drawn for the present investigation.

(1) The RJSB features more efficient air utilization and enhanced particle mixing and circulation when compared with conventional spouted beds.

(2) Operation of the RJSB is very flexible because of the adjustable rotational speed. The following three distinct flow regimes were identified:

1. Full rotating spouting (low rpm)
2. Rotating central spouting-pulsating annulus (moderate rpm)
3. No spouting with local pulsation; pseudo fluidization (high rpm)

(3) Adjustment of the rotational speed of the distributor provides a simple means to control particle circulation and turnover in the bed.

(4) The distributor rotational speed has a major effect on the spouting mechanism and the flow regimes. However, it has only a minor effect on the minimum spouting velocity and pressure drop values within the full spouting and the central spouting regimes.

(5) The minimum spouting Reynolds number varies almost linearly with the dimensionless bed height and nozzle diameter and with the square root of the Archimedes number.

(6) The RJSB has lower peak pressure drop but a comparable steady spouting pressure drop relative to the conventional spouted beds.

6. Nomenclature

Symbols

Ar	Archimedes number $= (D_p^3 \rho_g (\rho_s - \rho_g) g) / (\mu_g^2)$
B	Breadth (m)
D_c	Column diameter (m)
D_n	Nozzle diameter (m)
D_p	Effective particle diameter $= D_{pe} \times \phi$ (m)
D_{pe}	Equivalent spherical particle diameter (m)
D_{pgm}	Geometric mean particle diameter (m)
g	Acceleration of gravity (m/s^2)
H	Bed height (m)
L	Length (m)
N	Distributor rotational speed (rpm)
ΔP_{bed}	Bed pressure drop (Pa)
ΔP_M	Peak pressure drop (Pa)
ΔP_s	Steady spouting pressure drop (Pa)
Q_{ms}	Air flow rate at minimum spouting condition (m^3/s)
Re	Particle Reynolds number $= (D_p U \rho_g) / (\mu_g)$
U	Superficial air velocity based on the total flow in the bed (m/s)
U_{mf}	Minimum superficial air velocity for fluidization (m/s)
U_{ms}	Minimum superficial air velocity for spouting (m/s)
U_t	Particle terminal velocity (m/s)
V_θ	Air distributor circumferential velocity (m/s)
Z	Thickness (m)

Greek letters

ε	Voidage (−)
μ_g	Viscosity of gas (Pa s)
ρ_b	Bulk density (kg/m^3)
ρ_g	Gas density (kg/m^3)
ρ_s	Solid density (kg/m^3)
ϕ	Sphericity (−)

Subscripts and superscripts

o	Stationary nozzle
1	First or central region nozzle
2	Second or annular region nozzle
b	Bed, bulk
c	Column
g	Gas
mf	Minimum fluidization
ms	Minimum spouting
n	Nozzle
p	Particle
s	Solid
θ	Circumferential

References

[1] R.Y. Jumah, Flow and Drying Characteristics of a Rotating Jet Spouted Bed, PhD Thesis, McGill University, Montreal, 1995.

[2] K.B. Mathur, N. Epstein, Spouted Beds, Academic Press, New York, 1974.

[3] J. Nemeth, E. Pallai, E. Aradi, Scale-up examination of spouted bed dryers, Can. J. Chem. Eng. 61 (1983) 419–425.

[4] E. Pallai, J. Nemeth, E. Aradi, Development of spouted bed dryer, in: A.S. Mujumdar (Ed.), Drying '84, Hemisphere McGraw-Hill, New York, 1984, pp. 158–165.

[5] A.S. Mujumdar, Spouted bed technology—a brief review, in: A.S. Mujumdar (Ed.), Drying '84, Hemisphere McGraw-Hill, New York, 1984, pp. 151–157.

[6] M.L. Passos, A.S. Mujumdar, V.G.S. Raghavan, Spouted beds for drying: principles and design considerations, Chap. 7, in: A.S. Mujumdar (Ed.), Advances in Drying, Vol. 4, Hemisphere Publishing, New York, 1987, pp. 359–398.

[7] Mohsenin, Physical Properties of Plant and Animal Materials, Vol. 1, Structure, Physical Characteristics and Mechanical Properties, Gordon and Breach Science Publishers, New York, 1970.

[8] A. Haider, O. Levenspiel, Drag coefficients and terminal velocity of spherical and nonspherical particles, Powder Technol. 58 (1989) 63–70.

[9] D.C. Chitester, R.M. Kornosky, L.-S. Fan, J.P. Danko, Characteristics of fluidization at high pressure, Chem. Eng. Sci. 39 (1984) 253–261.

[10] D. Kunii, O. Levenspiel, Fluidization Engineering, Butterworth-Heinemann, Boston, 1991.

[11] S.J. Kline, F.A. McClintock, Describing uncertainties in single-sample experiments, Mech. Eng. 75 (1953) 3–9.

[12] R.J. Moffat, Describing uncertainties in experimental results, Exp. Thermal Fluid Sci. 1 (1988) 3–17.

[13] H. Schenck, Theories of Engineering Experimentation, 2nd edn., McGraw-Hill, New York, 1968.

[14] H. Becker, An investigation of laws governing the spouting of coarse particles, Chem. Eng. Sci. 13 (1961) 245–262.

[15] M. Anabtawi, B. Uysal, R. Jumah, Flow characteristics in a rectangular spout-fluid bed, Powder Technol. 69 (1992) 205–211.

[16] B. Ghosh, A study on the spouted bed—a theoretical analysis, Indian Chem. Eng. 7 (1995) 16.

[17] P. Chandnani, N. Epstein, Spoutability and spout destabilization of fine particles with a gas, in: K. Ostergaard, Sorensen (Eds.), Fluidization, Engineering Foundation, New York, 1986, pp. 233–240.

[18] R.Y. Jumah, A.S. Mujumdar, G.S.V. Raghavan, Batch drying kinetics of corn in a novel rotating jet spouted bed, Can. J. Chem. Eng. 74 (1996) 479–486.